Inorganic Chemistry

Article

pubs.acs.org/IC

Sonochemical Synthesis and Properties of Nanoparticles of $FeSbO_4$

Pratanu Nag,[†] Suparna Banerjee,[†] Yongmoon Lee,[‡] Ali Bumajdad,[§] Yongjae Lee,[‡] and P. Sujatha Devi*[,†]

[†]Nano-Structured Materials Division, CSIR-Central Glass and Ceramic Research Institute, Kolkata 700032, India

[‡]Department of Earth System Sciences, Yonsei University, Seoul, 120749, Korea

[§]Chemistry Department, Faculty of Science, Kuwait University, P.O. Box 5969, Safat 13060, Kuwait

ABSTRACT: A sonochemical method was employed to prepare reactive nanoparticles of $FeSbO_4$ at 300 °C, which is the lowest calcination temperature reported so far for preparing $FeSbO_4$. A systematic evolution of the $FeSbO_4$ phase formation as a function of temperature was monitored by in situ synchrotron X-ray measurements. The 300 and 450 °C calcined powders exhibited specific surface areas of 116 and 75 m^2/g, respectively. The X-ray photoelectron spectra analysis confirmed the presence of mainly Fe^{3+} and Sb^{5+} in the calcined powder. The response of the fabricated sensors (using both 300 and 450 °C calcined powders) toward 1000 ppm and 1, 2, 4, and 8% hydrogen, respectively, has been monitored at various operating temperatures. The sensors fabricated using 300 °C calcined powder exhibited a response of 76% toward 4% H_2 gas at an operating temperature of 300 °C, while those fabricated using 450 °C calcined powder exhibited a higher response of 91% with a quick recovery toward 4% H_2 gas at 300 °C. The results confirmed that a higher calcination temperature was preferred to achieve better sensitivity and selectivity toward hydrogen in comparison to other reducing gases such as butane and methane. The experimental results confirmed that the sonochemical process can be easily used to prepare $FeSbO_4$ nanoparticles for various catalytic applications as demonstrated. Here, we project $FeSbO_4$ as a new class of material exhibiting high sensitivity toward a wide range of hydrogen gas. Such sensors that could detect high concentrations of hydrogen may find application in nuclear reactors where there will be a leakage of hydrogen.

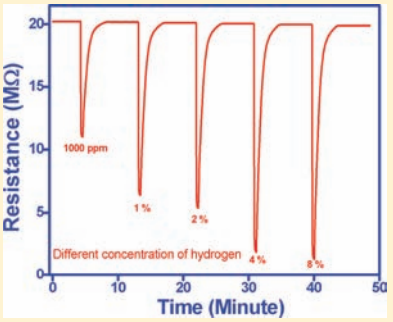

INTRODUCTION

$FeSbO_4$ is known to be an important catalytic material for the selective oxidation of hydrocarbons, such as alkanes and alkenes.[1] In spite of its interesting catalytic applications, there is relatively little work carried out on various other properties of this compound. To the best of our understanding, most of the studies on this compound have been focused mainly on its catalytic properties,[2−7] although a few are available on its magnetic and structural studies.[8−13] $FeSbO_4$ (squawcreekite) has the rutile structure with space group $P4_2/mnm$, where the Fe and Sb cations are randomly distributed in the 2a site, that is, in the octahedral sites within the oxygen lattice. Although different forms of Fe_2O_3 have been extensively studied as gas-sensing materials, such studies on $FeSbO_4$ have rarely been conducted.[14−16] Recently, Zhang et al. have reported the sensitive response to LPG by $FeSbO_4$-based materials with high sensitivity and selectivity as compared with SnO_2-based materials.[15,16] It is speculated that $FeSbO_4$-based materials may replace SnO_2-based sensors in the future.

Here, we report for the first time the sonochemical synthesis of $FeSbO_4$ nanoparticles and its gas-sensing characteristics toward H_2 gas. There has been a growing interest to develop simple processes for the preparation of nanoparticles of $FeSbO_4$ due to their diverse catalytic applications. The major processes available for the synthesis of $FeSbO_4$ have been limited to the solid state reaction method, mechanochemical method, and coprecipitation method.[15−18] Most of these methods are complex and require a high calcination temperature of 500−1100 °C for the phase formation, which make the quality of the prepared $FeSbO_4$ powders quite inferior. The only report on the low temperature synthesis of iron antimony oxide ($FeSbO_4$) with a specific surface area over 50 m^2/g was by a mechanochemical process by milling a mixture of iron oxyhydroxide (FeOOH) and antimony pentoxide (Sb_2O_5) using a planetary ball mill at room temperature.[17] The sonochemical process[19] has the potential to form fine complex oxides in a single and simple operation at room temperature followed by calcination at moderately lower temperatures. In this process, the acoustic cavitation (~5000 K, ~500 bar) generated during the irradiation of liquids with ultrasound creates transient local conditions, which can easily decompose the metal precursors to generate nanosized particles.

A gaseous hydrogen leakage of 4.65% (lower explosive limit, LEL) in oxygen and 4.0% in air, at normal conditions [at one atmospheric pressure (101.325 KPa) and room temperature (25 °C)], may lead to an explosive atmosphere of easy ignition.[20] As hydrogen is odorless, colorless, and tasteless and most human senses will not help to detect its leakage, it is essential to use hydrogen sensors for the detection of hydrogen leakage by means of developing sensitive, reliable, and cost-effective hydrogen sensors. Here, we have explored the capability of nanoparticles of $FeSbO_4$ to detect the presence of hydrogen from the ppm level to the percentage level. Such

Received: June 23, 2011
Published: December 27, 2011

sensors especially find applications in nuclear reactors and satellite launch pads.

EXPERIMENTAL SECTION

Preparation of $FeSbO_4$ Nanoparticles. All of the chemicals used were of AR grade. For a particular batch preparation, 0.2 M solutions each of iron(III) nitrate nonahydrate (Merck India Ltd., Mumbai) and antimony(III) oxide (99% purity, Merck India Ltd.) were prepared in a slightly acidic solution and mixed proportionately as per the requirement. The mixed solution was then sonicated (Ultrasonic processor, model-PR 1000) for 30 min followed by slow and dropwise addition of liquor NH_3 (35%, Merck India Ltd.) until the pH of the solution increased to 9−10 and complete precipitation occurred. The sonication was continued for another half an hour, and the warm suspension was allowed to cool down to room temperature. The brownish precipitate obtained was centrifuged and washed several times with distilled water and acetone in a sequence. The precipitate was finally air-dried and ground in a mortar and pestle before calcination at 300/450 °C for 6 h in air with a heating and cooling rates of 100 °C per hour to achieve the desired calcined oxide powders.

Characterization of $FeSbO_4$ Nanoparticles. The room temperature powder X-ray diffraction (XRD) were carried out on both the as-synthesized and the calcined powders for phase identification using a Philips X-ray diffractometer (PW1730) with Cu Kα radiation at a 2θ scan rate of 1° per minute. The crystallite size has been calculated from the X-ray line broadening using Scherrer's formula. In situ variable-temperature synchrotron X-ray powder diffraction experiments were performed at the 5A beamline at Pohang Accelerator Laboratory (PAL). An 18 keV synchrotron X-ray beam of 500 μm in diameter was provided by a sagitally focusing monochromator and mirrors. The as-prepared materials were packed into 0.7 mm diameter quartz capillaries. The capillaries were then wrapped with a heating coil for in situ variable-temperature experiments.[21] The temperature was increased continuously from room temperature to 590 °C, while the diffraction data were measured for 1 min on MAR345 imaging plate. The data were processed after detector calibration against LaB6 standard data using the Fit2d suite of programs.[22]

The specific surface area of the calcined powders was determined by BET method on a Quantachrome Instrument (NOVA 4000 E series). The particle size and the powder morphology of the calcined powders were determined with the help of a transmission electron microscope (TEM), JEOL (JEM-200X). X-ray photoelectron spectra (XPS) were recorded on a Thermo ESCALAB 250 Xi using Al Kα radiation (1486.6 eV). The spectra acquisition and processing were carried out using the software Thermo Avantage Version 4.58. The sample was introduced into the preparation chamber with the sample holder and degassed until a good vacuum was achieved. Then, it was transferred into the analysis chamber where the vacuum was 10^{-9}−10^{-10} mBar. The analyses were carried out with pass energy of 20 eV, a dwell time of 50 ms, and a step size of 0.1 eV. A flood gun using argon gas (99.9999% pure) and standard charge compensation mode was used to neutralize the charge build up, if any, on the surface of the samples. The binding energy standardization was achieved using silver sample ($Ag3d_{5/2}$ at 368.29 eV). The BE values were corrected with the contamination carbon (C1s at 284.60 eV).

Sensor Fabrication. The thick pastes of the 300 and 450 °C calcined $FeSbO_4$ powders have been made using alumina gel as a binder and then coated on the outer surface of several thin alumina tubes (length 3 mm, outer diameter 2 mm, and thickness 0.5 mm and coating thickness of 50−60 μm) with gold electrodes and platinum lead wires. The coatings have been cured at 450 °C for 45 min. The sensor units fabricated with 300 and 450 °C calcined iron antimonate were stabilized by heating continuously for 3−7 days before the measurement.[23]

The percent response or sensitivity (S) of the sensors fabricated from the synthesized $FeSbO_4$ powders toward different concentrations of hydrogen gas was determined using the following relation: $S\ (\%) = [R_A - R_G]/R_A \times 100$, where R_A is the sensor resistance in air at a particular temperature and R_G is the sensor resistance in hydrogen gas at the same temperature.

RESULTS AND DISCUSSION

Characterization of $FeSbO_4$ Nanoparticles. In Figure 1, XRD patterns of the as-prepared, 300 and 450 °C calcined

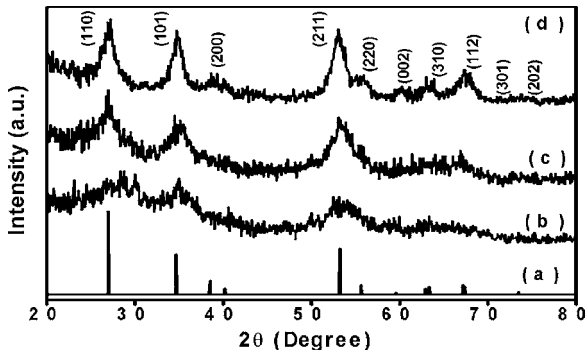

Figure 1. XRD patterns of the (a) JCPDS card no. 46-1387 of $FeSbO_4$, (b) as-prepared $FeSbO_4$, (c) 300 °C calcined $FeSbO_4$, and (d) 450 °C calcined $FeSbO_4$ powders.

$FeSbO_4$ nanocrystalline powders are compared with the reported data of $FeSbO_4$ (JCPDS card no. 46-1387). Even in the as-prepared form (Figure 1b), there is an indication of the formation of the $FeSbO_4$ phase. The 300 °C calcined powder exhibited all of the reflections of the $FeSbO_4$ phase as per the JCPDS pattern having the rutile type structure. It is important to note that although the XRD patterns of the 300 °C calcined powder were composed of well-defined reflections, they were very broad. The large widths of the diffraction peaks are due to the formation of finer crystallites in the sample. The broad peaks arise from the finite number of diffracting planes, and the extent of broadening was calculated using the Scherrer formula. The average crystallite sizes estimated from the full width half maxima data using Scherrer's formula were 3 and 5 nm, respectively, for the 300 and 450 °C calcined $FeSbO_4$ powders. Furthermore, no evidence of the presence of any other crystalline phases, such as $FeSb_2O_4$ or $FeSb_2O_6$, was seen in the XRD patterns. The XRD pattern confirms the complete formation of the rutile squawcreekite $FeSbO_4$ phase at 300 °C. In fact, a calcination temperature of 300 °C was the lowest to be reported so far in the literature for the preparation of nanoparticles of $FeSbO_4$. The calcined powders exhibited large surface area characteristics of nanocrystalline materials. The measured BET specific surface area was 116 and 75 m^2/g, respectively, for the 300 and 450 °C calcined powders.

Temperature-dependent changes of the XRD patterns of the as-prepared materials are illustrated in Figure 2. From Figure 2, it is clear that the formation of the $FeSbO_4$ rutile phase is almost complete around 300 °C, and above 350 °C, it is 100% rutile phase. There are no additional phases like FeO, Fe_2O_3, Sb_2O_3, Sb_2O_5, $FeSb_2O_4$, or $FeSb_2O_6$ present in the diffraction patterns. We also calculated the crystallite size from the high-resolution synchrotron data that have been recorded by in situ heating. The crystallite size has been calculated to be around 2.5 nm at 300 °C and 3 nm at 450 °C, respectively. As evident from Figure 2, we could not observe any major change in the crystallite size with temperature during in situ heating. As discussed earlier, there was a minor increase in the crystallite size for the ex situ-heated samples, probably due to the

dx.doi.org/10.1021/ic201353u | Inorg. Chem. 2012, 51, 844−850

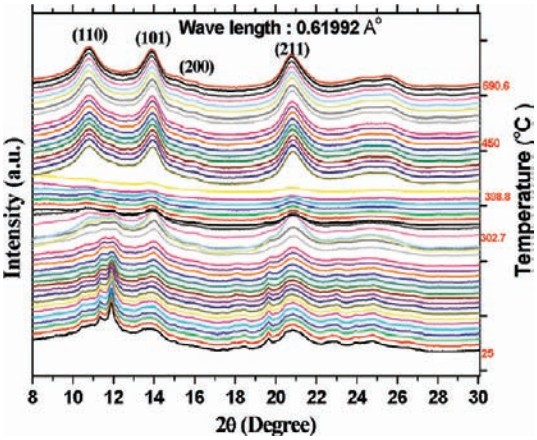

Figure 2. Time-resolved synchrotron X-ray powder diffraction patterns collected during the in situ heating of the as-prepared powder.

increased time available during calcination for the crystallites to grow in size. The lattice parameters and unit cell volumes calculated using the synchrotron data are plotted as a function of temperature in Figure 3. A minor decrease in the "a" value and an increase in the "c" value was noticed as compared to the

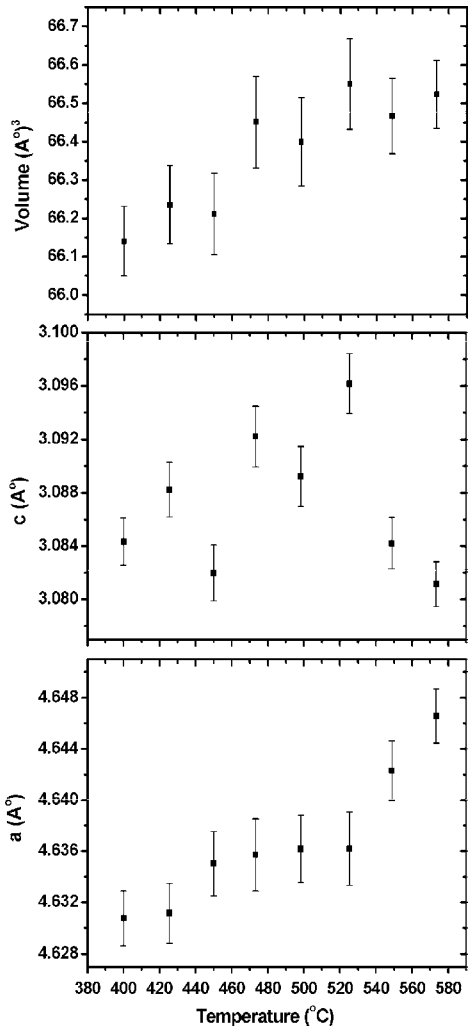

Figure 3. Variation of the unit cell volume and lattice parameters with temperature calculated from the synchrotron X-ray data.

reported values. Overall, the $FeSbO_4$ rutile phase exhibited normal thermal expansion behavior up to the final temperature of 590 °C.

In Figure 4a–d, the TEM pictures and the corresponding HRTEM images of the 300 and 450 °C calcined $FeSbO_4$ powders, respectively, are shown. The TEM pictures of 300 °C calcined $FeSbO_4$ powder confirm the formation of highly agglomerated particles consisting of fine crystallites of sizes below 5 nm, which matches well with the size calculated from the XRD analysis of the powders. The 300 °C calcined $FeSbO_4$ powder, due to the finer size and high surface area, exhibited particle agglomeration, whereas with an increase in calcination temperature from 300 to 450 °C, the initially formed crystallites aggregate further to form slightly larger aggregates as clearly observed from the TEM pictures in Figure 4c. However, with an increase in calcination temperature from 300 to 450 °C, not much increase in the crystallite size was evident in the HRTEM pictures (Figure 4b,d). For the 450 °C sample, the crystallite size calculated from the XRD line broadening was almost identical to that of the majority of the particles seen in the TEM photographs, indicating that each particle viewed under TEM was a single crystal.

To get insight into the oxidation states of Fe and Sb, which are suppose to have trivalent and pentavalent oxidation states in iron antimonate, in Figure 5a–d, the Fe2p and Sb3d+O1s spectra collected from the 300 and 450 °C calcined $FeSbO_4$ samples are presented. The binding energy peaks of $Fe2p_{3/2}$ and $Fe2p_{1/2}$ for the 300 °C calcined sample were found at 711.4 and 724.6 eV, respectively. Similarly, for the 450 °C calcined sample, the Fe2p energy bands were located at 711.4 and 724.9 eV, respectively. Fe(III) has a $Fe2p_{3/2}$ binding energy of 711.2 eV in all iron oxides, and Fe(II) has a binding energy of 709.7 eV in Fe_xO.[24,25] Because the main signals were broad and asymmetric, it was very difficult to distinguish the presence of Fe^{3+} and Fe^{2+} in our samples. Therefore, we have deconvoluted the XPS signals very carefully. The main peaks were accompanied by satellite structures as evident in Figure 5a,c. The broad satellite signal centered at 719.3 (Figure 5a) and 719.1 eV (Figure 5c), respectively, for the 300 and 450 °C calcined samples is characteristic of the presence of Fe(III) in our samples. Furthermore, the absence of a satellite signal at 715 eV confirms the absence of Fe(II) in the calcined samples. The above results confirm the presence of only Fe^{3+} in the calcined $FeSbO_4$ powder samples. We also analyzed the oxidation states of antimony in both the 300 and the 450 °C calcined powders. For the 300 °C calcined sample (Figure 5b), the binding energy peaks of $Sb3d_{5/2}$ were observed at 528.4 eV, corresponding to Sb^0, and at 531.2 eV, corresponding to Sb^{5+}, respectively. Similarly, the $Sb3d_{3/2}$ band can be separated into two Gaussian peaks, one at 540.5 eV corresponding to Sb^{5+} and the other at 537.5 eV corresponding to Sb^0.[26,27] Although the XPS results confirmed the presence of both Sb^0 and Sb^{5+} on the surface of the 300 °C calcined powder, the majority of the ions were in the Sb^{5+} state only. The O1s peak could clearly be seen at 530.2 and 530.1 eV, respectively, for the 300 and 450 °C samples.[27−29] As compared to 300 °C calcined powder, zerovalent antimony was absent in the 450 °C calcined $FeSbO_4$ powder. However, a shift in the BE was noticed from 531.2 eV to a lower value of 530.7 eV (see Figure 5d) for the 450 °C calcined sample. The binding energies of Sb^{3+} and Sb^{5+} are very close to each other, and the Sb^{5+} binding energy was reported to be in the range of 530.6–530.9 eV.[28] However, the BE of Sb^{3+} was also assigned around 530.6 eV. Therefore, we

dx.doi.org/10.1021/ic201353u | Inorg. Chem. 2012, 51, 844–850

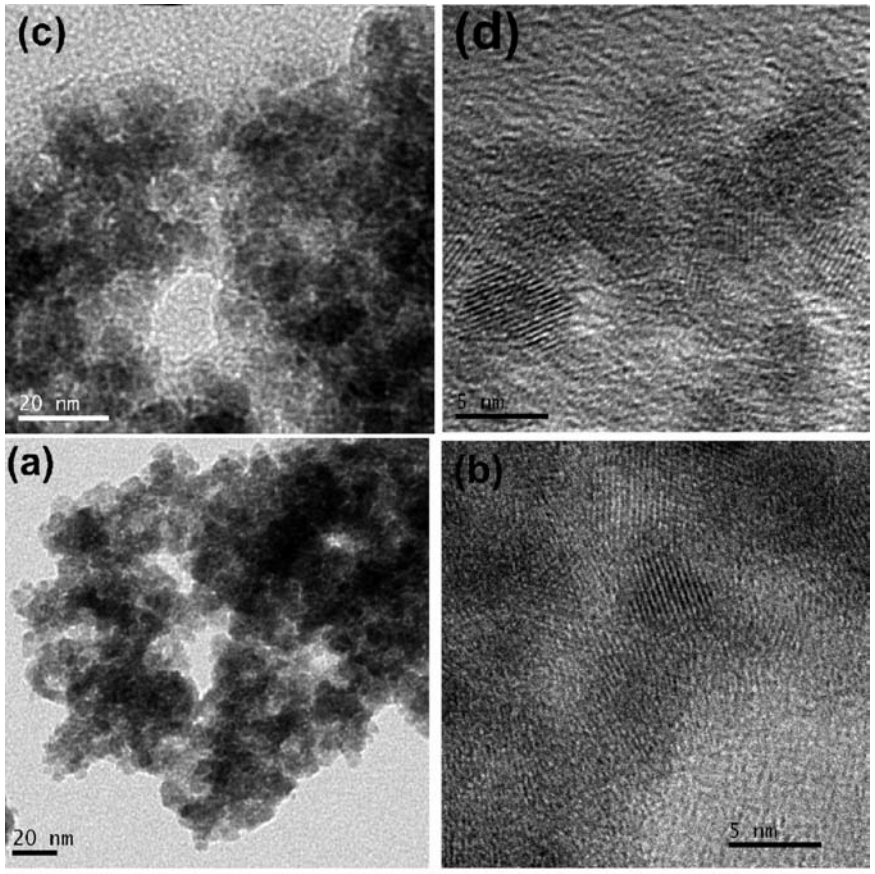

Figure 4. (a) TEM and (b) HRTEM pictures of the 300 °C and (c) TEM and (d) HRTEM pictures of the 450 °C calcined $FeSbO_4$ powders.

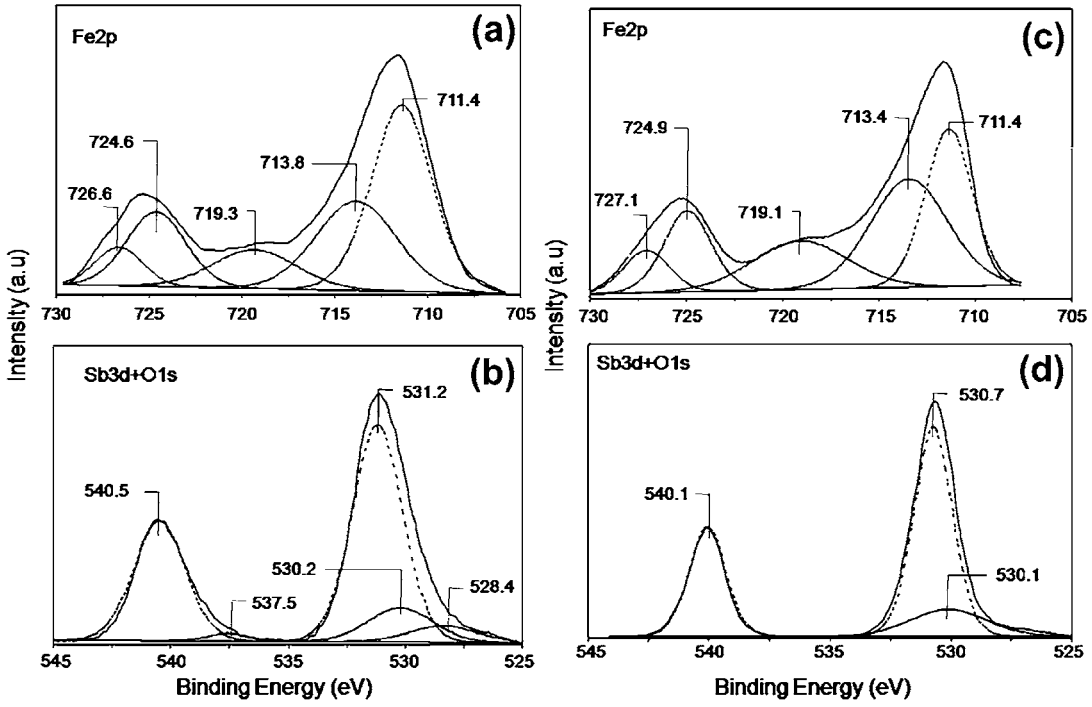

Figure 5. XPS data collected from the 300 (a and b) and 450 °C (c and d) calcined $FeSbO_4$ powder samples.

anticipated the presence of a small amount of Sb^{3+} giving rise to a shift in the BE energy of Sb. We still believe that in the 450 °C sample Sb is present mainly in the pentavalent form. The O/Sb ratio for the 300 °C calcined sample was 3.1, while for the 450 °C calcined sample, it was 4.17.

Gas-Sensing Properties. The characteristics of the sensors fabricated using 300 and 450 °C calcined $FeSbO_4$ powders have

dx.doi.org/10.1021/ic201353u | *Inorg. Chem.* 2012, 51, 844–850

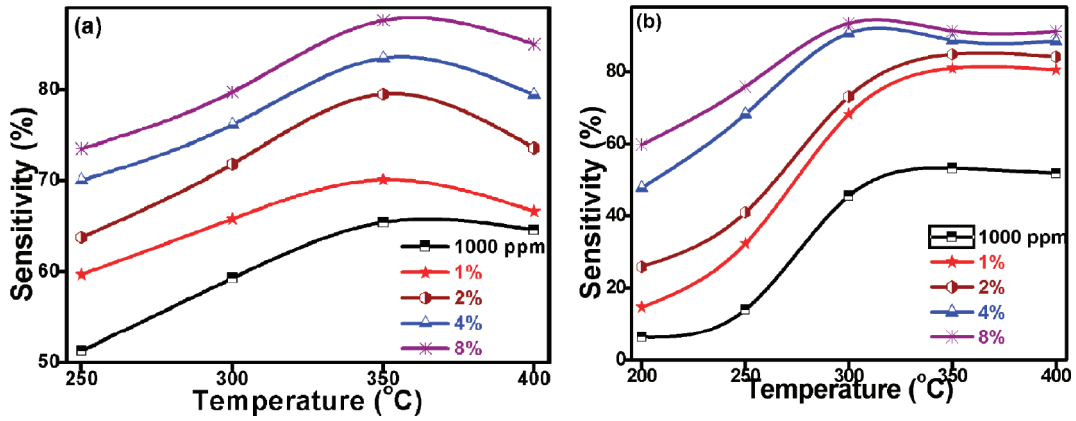

Figure 6. Percentage response characteristics as a function of temperature toward different concentrations of H_2 gas exhibited by the sensors fabricated using (a) 300 and (b) 450 °C calcined $FeSbO_4$ powder.

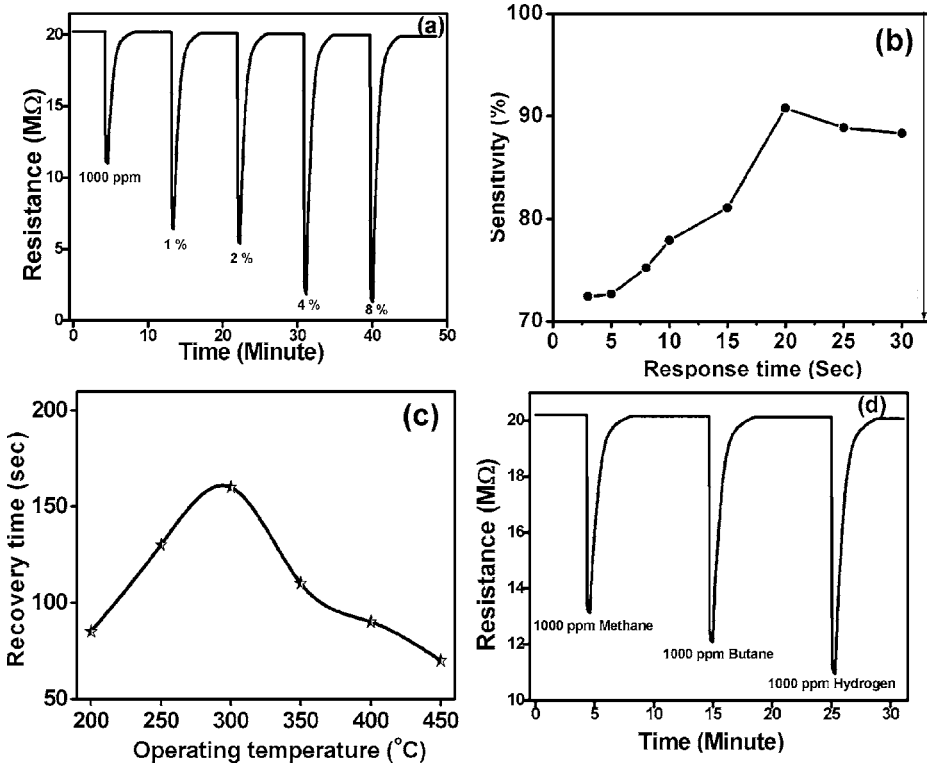

Figure 7. Various response characteristics of the sensor fabricated using 450 °C calcined $FeSbO_4$ powder. (a) Dynamic response curve recorded at 300 °C at different concentrations of hydrogen, (b) variation of sensitivity with response time toward 4% H_2 gas, (c) variation of recovery time with operating temperature toward 4% H_2 gas, and (d) response toward 1000 ppm methane, butane, and hydrogen gas at 300 °C.

been monitored at various gas concentrations from 1000 ppm to a higher concentration of 8% H_2. In Figure 6a,b, the percentage response as a function of temperature toward different H_2 gas concentrations (e.g., 1000 ppm and 1, 2, 4, and 8%) is plotted for both of the sensors. At an operating temperature of 350 °C, the 300 °C sensor exhibited a response of 65 and 80% toward 1 and 2% H_2 gas, respectively. On exposure of the senor to 4% H_2 gas for 20 s, the sensor resistance in air dropped drastically, resulting in a high sensitivity of 83.5%. Toward 8% H_2 gas, the response increased to 87.6% at 350 °C. At all temperatures, the sensitivity increased linearly with gas concentration, reaching a maximum at 350 °C and then decreasing. Even at lower operating temperatures of 250 and 300 °C, the response of the same sensor toward 4% H_2 gas was around 70 and 76%, respectively. Although the sensor fabricated using 300 °C calcined $FeSbO_4$ powder exhibited a higher sensitivity, because of the high resistance of the sensor in air, the detailed studies have been carried out only on those fabricated using 450 °C calcined $FeSbO_4$ powder. Such sensors exhibited 90.8% sensitivity toward 4% hydrogen at an operating temperature of 300 °C. It is interesting to note that the sensors fabricated using 450 °C calcined powder exhibited a maximum response at 300 °C. Beyond 350 °C, saturation in the response data has been observed (see Figure 6b). Toward exposure to 8% H_2 gas, these sensors were highly responsive and exhibited 93.5% sensitivity at 300 °C.

Figure 7a–d shows the various response characteristics of the sensor fabricated using 450 °C calcined $FeSbO_4$ powder. In Figure 7a, the dynamic response curve recorded for the 450 °C

dx.doi.org/10.1021/ic201353u | *Inorg. Chem.* 2012, 51, 844–850

sensor at 300 °C for various concentrations of hydrogen is presented. In Figure 7b, the variation of sensitivity with response time is plotted. The percentage sensitivity increased linearly from 72.42 to 91% when the response time was varied from 3 to 20 s. In Figure 7c, the variation of recovery time with operating temperature is plotted. The recovery time was highest at 300 °C and finally decreased to 70 s at 450 °C. In Figure 7d, the response of the same $FeSbO_4$ sensor toward same concentrations (1000 ppm) of reducing gases at 300 °C is shown. Very low sensitivities of 40.04 and 35.0% toward 1000 ppm *n*-butane and 1000 ppm methane gases, respectively, were found as compared to a slightly higher sensitivity of 45.54% toward 1000 ppm hydrogen. A very low sensitivity of 49.10% toward 5000 ppm *n*-butane was found as compared to the high sensitivity of 90.8% toward 4% hydrogen. The corresponding selectivity coefficients $\beta = S_{H2}/S_{gas}$ calculated were 2.27 β = S(4% hydrogen/1000 ppm butane), 2.6 β = S(4% hydrogen/1000 ppm methane), 1.30 β = S(1000 ppm hydrogen/1000 ppm butane), and 1.14 β = S(1000 ppm hydrogen/5000 ppm butane) for this sensor. The same sensor was also selective toward hydrogen gas at 350 °C (53.22 and 88.8% toward 1000 ppm and 4% hydrogen gas, respectively) as compared to very low sensitivities of 42.11, 54.4, and 39.4% toward 1000 ppm *n*-butane, 5000 ppm *n*-butane, and 1000 ppm methane gases, respectively, with corresponding selectivity coefficients of 1.26 β = S(1000 ppm hydrogen/1000 ppm butane), 2.11 β = S(4% hydrogen/1000 ppm butane), 1.35 β = S(1000 ppm hydrogen/1000 ppm butane), and 2.26 β = S(4% hydrogen/1000 ppm methane), respectively. The sensor fabricated using the 300 °C calcined powder showed slightly higher sensitivities of 47.3, 56.2, and 44.8% toward 1000 ppm *n*-butane, 5000 ppm *n*-butane, and 1000 ppm methane gases, respectively, at 350 °C as compared to the sensor fabricated using the 450 °C calcined powder. The corresponding selectivity coefficients were 1.38 β = S(1000 ppm hydrogen/1000 ppm butane), 1.76 β = S(4% hydrogen/1000 ppm butane), 1.46 β = S(1000 ppm hydrogen/1000 ppm methane), and 1.86 β = S(4% hydrogen/1000 ppm methane), respectively, for this sensor. The above results indicate a better selectivity toward H_2 gas in comparison to other reducing gases like methane and butane at different temperatures. Contrary to the reports on $FeSbO_4$ exhibiting high sensitivity toward LPG gas,[15,16] the sensors fabricated using nanoparticles of $FeSbO_4$ exhibited excellent H_2-sensing properties, with poor response toward other reducing gases such as butane and methane.

The gas-sensing mechanism of a semiconductor depends on the reactions occurring on the surface of the particles. Normally, the atmospheric oxygen is chemisorbed on the sensor surface, consuming free electrons from the conduction band, resulting in an electron-depleted surface layer and a consequent rise in the resistance of the sensor.[30] It is assumed that when the nanocrystalline $FeSbO_4$ semiconductor film is exposed to air, physisorbed oxygen molecules pick up electrons from the conduction band of $FeSbO_4$ forming O_2^-(ads) and O^-(ads) species on the surface as shown below.

$$O_2(gas) + e^- = O_2(ads)^- \quad (1)$$

$$O_2(ads)^- + e^- = 2O(ads)^- \quad (2)$$

The interactions that probably could happen between adsorbed O_2^- and O^- ions (on the $FeSbO_4$ surface) and hydrogen (target gas) are given below in eqs 3 and 4:

$$2H_2 + O_2^-(ads) = 2H_2O + e^- \quad (3)$$

$$H_2 + O^-(ads) = H_2O + e^- \quad (4)$$

In addition to the surface reactions as depicted above, an oxide such as $FeSbO_4$ could also exhibit gas-sensing characteristics since it contains easily reducible multivalent ions such as Fe^{3+} and Sb^{5+}. In the presence of a reducing gas such as H_2, as per the redox reactions 5 and 6 shown below, reduction of Fe^{3+} to Fe^{2+} and Sb^{5+} to Sb^{3+} could occur resulting in the oxidation of H_2 to H_2O, thereby causing a reduction in the sensor resistance.

$$2Fe^{III}Sb^{V}O_4 + H_2(gas) \rightarrow H_2O + 2Fe^{III}Fe^{II}Sb^{V}O_4 \quad (5)$$

$$Fe^{III}Sb^{V}O_4 + H_2(gas) \rightarrow H_2O + 2Fe^{III}Fe^{II}Sb^{V}Sb^{III}O_4 \quad (6)$$

The corresponding redox potentials of the two different redox couples, namely, Fe^{3+}/Fe^{2+} and Sb^{5+}/Sb^{3+}, are shown in eqs 7 and 8, respectively.[31]

$$Fe^{III}{}_2O_3 + 2e^- \rightarrow 2Fe^{II}O + 0.5O_2 + V_o \quad (7)$$

where E° Fe^{3+}/Fe^{2+} = 0.771 V

$$Sb^{V}{}_2O_5 + 2e^- \rightarrow Sb^{III}{}_2O_3 + O_2 + 2V_o \quad (8)$$

where E° Sb^{5+}/Sb^{3+} = 0.649 V, which indicate that both Fe^{3+} and Sb^{5+} are strong oxidants, and in addition to the adsorbed oxygen ions (O^{2-} or O_2^-) on the $FeSbO_4$ sensor surface, these ions also facilitate the oxidation of the H_2 gas. Because E° (Fe^{3+}/Fe^{2+}) is greater than E° (Sb^{5+}/Sb^{3+}), Fe^{3+} is a stronger oxidizing agent with better tendency of reduction than Sb^{5+}. Hence, reaction 7 is expected to be favored in calcined $FeSbO_4$ powders, resulting in a much faster response and better gas-sensing properties. We believe that both the adsorption of O_2^- and O^- ions on the nanocrystalline $FeSbO_4$ surface and the ease of reduction of Fe^{3+} to Fe^{2+} are responsible for the response of $FeSbO_4$ nanoparticles toward H_2 gas.

CONCLUSIONS

In conclusion, a simple sonochemical method was successfully employed to prepare nanoparticles of $FeSbO_4$ at 300 °C. Temperature-dependent changes of the synchrotron X-ray powder diffraction patterns illustrated the disappearance of the starting phases completely at 300 °C, followed by the formation of $FeSbO_4$ rutile phase. The XPS analysis confirmed the presence of Fe^{3+} and Sb^{5+} as the major valence states in the calcined samples. A sensor fabricated using 450 °C calcined $FeSbO_4$ powder was better in terms of R_{air}, percent sensitivity, recovery time, response time, and reproducibility. These sensors exhibited better and faster response (91% for 20 s) and quick recovery toward 4% H_2 gas at a low operating temperature of 300 °C. Contrary to the reports on $FeSbO_4$ exhibiting high sensitivity toward LPG gas, the sensors fabricated using nanoparticles of $FeSbO_4$ exhibited excellent H_2-sensing properties, with poor response toward other reducing gases such as butane and methane. The experimental results thus indicate that this simple and cost-effective sonochemical process can be used to prepare $FeSbO_4$ nanoparticles to use them as potential hydrogen gas sensor material. Such sensors that could detect high concentrations of

dx.doi.org/10.1021/ic201353u | *Inorg. Chem.* 2012, 51, 844–850

hydrogen could find applications in nuclear reactors, where there will be a huge leakage of hydrogen.

AUTHOR INFORMATION

Corresponding Author

*E-mail: psujathadevi@cgcri.res.in or psujathadevi@gmail.com.

ACKNOWLEDGMENTS

P.S.D. acknowledges the financial support from Board of Research in Nuclear Sciences (BRNS). P.S.D. also acknowledges the cooperation of the members of the Sensor and Actuator Division during the course of this work. The assistance of the technical unit of SAF (GS01/01) of Kuwait University is acknowledged. Y.L. is thankful for the support from the Global Research Laboratory program of the National Research Foundation and the BK21 program of the NRF to the Institute of Earth, Atmosphere, and Astronomy at Yonsei University. Experiments at PAL were supported in part by the MEST and Pohang University of Science and Technology (POSTECH).We greatly appreciate the critical comments and constructive suggestions of the anonymous reviewers that helped us to improve the manuscript.

REFERENCES

(1) Keulks, G. W.; Lo, M. Y. *J. Phys. Chem.* **1986**, *90*, 4768.
(2) Allen, M. D.; Bowker, M. *Catal. Lett.* **1995**, *33*, 269.
(3) Carrazán, S. R. G.; Cadus, L.; Dieu, P.; Ruiz, P.; Delmon, B. *Catal. Today* **1996**, *32*, 311.
(4) Castillo, R.; Dewaele, K.; Ruiz, P.; Delmon, B. *Appl. Catal.* **1997**, *153*, L1.
(5) Fattore, V.; Fuhran, Z.; Manara, G.; Notari, B. *J. Catal.* **1975**, *37*, 223.
(6) Steen, E. V.; Schnobel, M.; Walsh, R.; Riedel, T. *Appl. Catal.* **1997**, *165*, 349.
(7) Magagula, Z.; Steen, E. V. *Catal. Today* **1999**, *49*, 155.
(8) Bithell, E. G.; Doole, R. C.; Goringe, M. J.; Allen, M. D.; Bowker, M. *Phys. Status Solidi* **1994**, *146*, 461.
(9) Crespo, R. G.; Leeuw de, N. H.; Catlow, C. R. A. *J. Mater. Chem.* **2003**, *13*, 2848.
(10) Crespo, R. G.; Moreira, I. D. R.; Illas, F.; Leeuw de, N. H.; Catlow, C. R. A. *J. Mater. Chem.* **2006**, *16*, 1943.
(11) Crespo, R. G.; Leeuw de, N. H.; Catlow, C. R. A. *Chem. Mater.* **2004**, *16*, 1954.
(12) Martinelli, A.; Ferretti, M.; Buscaglia, V.; Cabella, R.; Lucchetti, G. *J. Therm. Anal. Calorim.* **2002**, *70*, 123.
(13) Walczak, J.; Felipek, E.; Bosacka, M. *Solid State Ionics* **1997**, *103*, 1363.
(14) Nakatani, Y.; Matsuoka, M. *Jpn. J. Appl. Phys.* **1983**, *22*, 233.
(15) Zhang, T.; Zhang, R.; Zhang, J.; Li, Y.; Hing, P. *J. Mater. Res.* **2000**, *15*, 2356.
(16) Zhang, T.; Hing, P. *J. Mater. Sci., Mater. Electron.* **1999**, *10*, 509.
(17) Tojo, T.; Zhang, Q.; Saito, F. *Powder Technol.* **2008**, *181*, 281.
(18) Martinelli, A.; Ferretti, M. *Mater. Res. Bull.* **2003**, *38*, 1629.
(19) Suslick, K. S. *Science* **1990**, *247*, 1439.
(20) Lewis, B.; von Elbe, G. In *Handbook of Chemistry and Physics*, 58th ed.; Weast, R. C., Ed.; CRC Press: Cleveland, OH, 1977−1978; pp 107−108.
(21) Stahl, K.; Hanson, J. C. *J. Appl. Crystallogr.* **1994**, *27*, 543.
(22) Hammersley, A. P.; Svensson, S. O.; Hanfland, M.; Fitch, A. N.; Hausermann, D. *High Pressure Res.* **1996**, *14*, 235.
(23) Banerjee, S.; Bumajdad, A.; Devi, P. S. *Nanotechnology* **2011**, *22*, 275506.
(24) Graat, P. C. J.; Somers, M. A. J. *Appl. Surf. Sci.* **1996**, *100−101*, 36.
(25) Kuivila, C. S.; Butt, J. B.; Stair, P. C. *Appl. Surf. Sci.* **1988**, *32*, 99.
(26) Castro, C. S.; Oliveira, L. C. A.; Guerreiro, M. C. *Catal. Lett.* **2009**, *133*, 41.
(27) Berry, F. J.; Holden, J. G.; Loretto, M. H. *J. Chem. Soc., Dalton Trans.* **1987**, 1727.
(28) Krishnakumar, T.; Jayaprakash, R.; Pinna, N.; Phani, A. R.; Passacantando, M.; Santucci, S. *J. Phys. Chem. Solids* **2009**, *70*, 993.
(29) Burriesci, N.; Garbassi, F.; Petrera, M.; Petrini, G. *J. Chem. Soc., Faraday Trans.* **1982**, *78*, 817.
(30) Frank, M. E.; Koplin, T. J.; Simon, U. *Small* **2006**, *2*, 36.
(31) Vanýsek, P. In *Handbook of Chemistry and Physics*, 75th ed.; Lide, D. R., Ed.; CRC Press: Boca Raton, FL, 1994−1995; pp 21−26.

NOTE ADDED AFTER ASAP PUBLICATION

This paper was published on the Web on December 27, 2011. Additional minor text corrections were made and the corrected version was reposted on December 29, 2011.